XFEM-Oriented Finite Element Parametric Analysis of CFRP-Retrofitted Concrete Beams Subjected to Center-Point Load

Taghi Mofid [1*], Ahmed Al-sharea [2]

[1] Assistant Professor, Department of Civil Engineering, Urmia University of Technology, Urmia, Iran

[2] Master's graduate, Department of Civil Engineering, Urmia University of Technology, Urmia, Iran

[*]Corresponding Author: Mofid.t@uut.ac.ir

[*]Corresponding Author ORC ID : https://orcid.org/0000-0002-0498-2553

Received: 03/01/2026
Revised: 02/05/2026
Accepted: 30/06/2026

Abstract

Retrofitting existing concrete buildings is vital. Using Fiber-Reinforced Polymer (FRP) composites, especially Carbon FRP (CFRP), significantly improves structural performance. The eXtended Finite Element Method (XFEM) is a superior modeling tool for such retrofitted structures, offering precision. This study uses XFEM in Abaqus to parametrically analyze CFRP-retrofitted concrete beams under flexure. Key examined parameters are concrete compressive strength (20-60 MPa), CFRP sheet thickness (0.1-0.2 mm), and the notch-to-beam height ratio (0.2-0.4). Results show that beams with lower concrete strength (20 MPa) exhibit 59% lower load capacity compared to higher strength concrete (60 MPa). Increasing CFRP thickness from 0.1 mm to 0.2 mm increases ultimate load by 68% and ductility index by 55%. While the first maximum load is minimally affected by CFRP thickness and depends on the concrete, the ultimate load increases sharply with thicker CFRP, indicating that the ultimate load is critically linked to CFRP activation after concrete cracking. Furthermore, increasing notch height from 40 mm to 60 mm reduces the first maximum load by 34% but affects the ultimate load by only 9%. In conclusion, CFRP retrofitting effectiveness is highly influenced by material and geometric properties, with XFEM providing accurate behavioral predictions for optimized strengthening designs.

Keywords: Retrofitting; Concrete Beam; Crack-Mouth Opening Displacement (CMOD); Extended Finite Element Method (XFEM); Abaqus.

1. Introduction

Retrofitting existing concrete structures has become increasingly important in the field of civil engineering due to a variety of factors (Jahami & Issa, 2024; Samadvand & Dehestani, 2020; Tran et al., 2025; Zhang et al., 2026). One key reason for the importance of retrofitting is the aging infrastructure in many cities around the world. As concrete structures age, they can deteriorate and become weakened, leading to potential safety hazards for occupants and pedestrians. Retrofitting allows for the reinforcement and strengthening of these structures, helping to extend their lifespan and ensure their continued functionality (Bai et al., 2024; DEHESTANI, 2020; Harle, 2024). Additionally, retrofitting can also improve the structural integrity of concrete buildings to better withstand natural disasters such as earthquakes (Kim & Kim, 2024; Ma et al., 2025; Mercimek et al., 2025). This is particularly crucial in regions prone to such events, where retrofitting can help mitigate the impact of these disasters and protect lives and property.Fiber Reinforced Polymer (FRP) composite materials have gained significant attention in retrofitting techniques due to their numerous advantages (Ashteyat et al., 2024; Cazacu et al., 2024; Satyanarayana, 2025). One key advantage is their high strength-to-weight ratio. This allows increasing the load-carrying capacity of a structure without adding excessive weight (Han et al., 2024; Hu et al., 2024; Saeidi Googarchin & Bidadi, 2025). This feature is particularly beneficial when the goal is to enhance structural performance without causing additional stress on the original structure. Additionally, FRP composites have excellent corrosion resistance. This makes them ideal for retrofitting projects in corrosive environments where traditional materials may deteriorate over time (SD & Pratap, 2025; Zhang et al., 2025; Zhang et al., 2024)Furthermore, FRP composites offer superior durability and longevity compared to traditional materials such as steel or concrete. This increased durability extends the service life of retrofitted structures, reducing the need for frequent maintenance. FRP composites are also non-corrosive, non-conductive, and non-magnetic. These properties make them attractive for retrofitting concrete structures in sensitive environments such as hospitals, laboratories, or power plants (Jahami & Issa, 2024; Tran et al., 2025). In summary, the advantages of FRP composites make them a versatile and cost-effective solution for enhancing the performance and longevity of existing structures.

2. Literature Review

The use of Carbon Fiber Reinforced Polymer (CFRP) as a strengthening material for concrete structures has gained significant attention among researchers in recent years. This is particularly important because concrete structures are increasingly exposed to severe environmental conditions and seismic events that accelerate their deterioration, compromising their load-bearing capacity and safety(Mofid & Tavakoli, 2020; Mofid & Tavakoli, 2021, 2023). Sakbana and Mashreib (Sakbana & Mashreib, 2020) conducted a study on the finite element analysis (FEA) of CFRP-reinforced concrete beams, aiming to evaluate the effectiveness of CFRP laminates in enhancing the structural performance of RC beams. They utilized the ABAQUS program to analyze key parameters such as load-deflection behavior, crack patterns, mid-span strain distribution, and failure modes. The study revealed that increasing the CFRP length from 600 mm to 900 mm enhanced beam capacity by approximately 13%, while extending it further to 1200 mm resulted in a 26% improvement. Additionally, increasing the CFRP thickness from 0.11 mm to 0.5 mm led to a 48% increase in both stiffness and flexural capacity. The study conducted by Paul and Sahu (Paul & Sahu, 2020) focused on the FEA of retrofitting reinforced concrete (RC) beams with CFRP plates using ABAQUS software. The research aimed to develop and validate FEA models for CFRP-strengthened RC beams, simulate the behavior of retrofitted beams under static loads, and investigate the impact of CFRP length on load-carrying capacity. The study utilized ABAQUS for modeling, incorporating key elements such as concrete with a plastic damage model, steel reinforcement with an elastic-perfectly plastic model, and CFRP with two material models. The results showed that increasing CFRP length led to enhanced load capacity. The comparison between isotropic and orthotropic CFRP models revealed minimal differences in load capacity. It was also concluded that CFRP retrofitting significantly improved RC beam performance, with longer CFRP plates providing greater strength, while the plastic damage model in ABAQUS effectively simulated concrete behavior, including cracking. Li et al. (Li et al., 2014) conducted a study on the three-point bending behavior of CFRP-reinforced concrete beams with initial cracks. They employed numerical simulations using XFEM within ABAQUS software to analyze crack propagation and the overall performance of the beams. The results indicated that CFRP reinforcement significantly enhanced the load-bearing capacity of the beams, demonstrating greater strength and improved structural integrity even in the presence of initial cracks. The findings emphasized the effectiveness of CFRP in mitigating the effects of cracking and improving the durability of concrete structures. Hosseini et al. (Hosseini et al., 2016) performed a numerical analysis of RC beams featuring both bending and shear openings, which were strengthened with FRP sheets. Utilizing FEM, they investigated the beam performance under various loading conditions. The results revealed that the application of FRP sheets significantly improved the load capacity and overall structural performance of the beams, effectively mitigating the negative effects of the openings. The study concluded that FRP strengthening is an effective method for enhancing the durability and safety of RC structures with structural weaknesses due to openings. Benaoum et al. (Benaoum et al., 2020) analyzed pre-cracked RC beams that were reinforced with composite materials. They utilized FEM to examine the performance of these beams under various loading conditions, focusing on crack propagation and structural integrity. The findings demonstrated that incorporating composite materials significantly enhanced the load-carrying capacity and improved the durability of the pre-cracked beams. The study concluded that the use of composite reinforcements effectively mitigated the effects of pre-existing cracks, reinforcing the structural resilience of concrete beams and providing a viable solution for strengthening damaged concrete structures. Salih and Zhou (Salih & Zhou, 2019) numerically investigated the behavior of RC beams reinforced with FRP bars. Using finite element analysis, they explored the performance of these beams under various loading conditions, focusing on aspects like load capacity, deflection, and stress distribution. The results indicated that beams reinforced with FRP bars exhibited enhanced load-carrying capacity compared to traditional steel reinforcement. The study concluded that FRP bars serve as an effective alternative for reinforcing concrete beams, particularly in environments prone to corrosion, thereby improving the longevity and durability of concrete structures. Sinaei et al. (Sinaei et al., 2011) carried out a numerical investigation on exterior RC beam-column joints strengthened with CFRP. Employing FEM, they analyzed the structural behavior of the joints, focusing on aspects such as load capacity, ductility, and failure modes. The findings revealed that the application of CFRP significantly enhanced the strength and performance of the beam-column joints, improving their resistance to shear and flexural forces. The study concluded that CFRP strengthening effectively mitigates vulnerability in beam-column joints, making it a viable solution for enhancing the structural integrity of RC structures. Shardakov et al. (Shardakov et al., 2016) examined the process of cracking in RC beams through both simulation and experimental methods. They utilized finite element analysis to model the cracking behavior of the beams and compared their results with experimental data. The study highlighted the mechanisms of crack formation and propagation, revealing that numerical simulations effectively captured the critical stages of cracking behavior. The findings emphasized the importance of understanding cracking processes to improve the design and durability of RC structures, ultimately contributing to enhanced safety and performance. Duarte et al. (Duarte et al., 2014) had an experimental and numerical investigation on the effect of repairing cracked RC beams strengthened with CFRP laminates. The research involved testing various beams to assess their performance before and after the application of CFRP laminates. The numerical models, developed using FEM, simulated the beam behavior under loading conditions, allowing for comparisons with experimental results. The findings indicated that the application of CFRP significantly enhanced the stiffness of the repaired beams. The study concluded that CFRP laminates are an effective solution for repairing and strengthening cracked RC beams, improving their structural performance and durability. Fan et al. (Fan et al., 2025) performed a numerical simulation study on the fracture process of CFRP-reinforced concrete. Employing advanced FEM techniques, they examined the fracture behavior and load response of CFRP-reinforced concrete under various loading conditions. The simulations could successfully capture crack initiation and propagation mechanisms, as well as the overall structural performance of the CFRP-reinforced beams. The findings indicated that CFRP reinforcement significantly improved the fracture resistance and load-bearing capacity of concrete structures. The study concluded that understanding the fracture process in CFRP-reinforced concrete is essential for developing effective design strategies to enhance the durability and performance of these materials in construction applications. Despite the studies conducted on retrofitting concrete structures with FRP composites, further examination on using XFEM approach to address load-crack-mouth opening displacement (CMOD) behavior of such reinforced members is necessary.

Several studies have specifically employed XFEM for fracture analysis of FRP-strengthened concrete members. For instance, (Esna Ashari & Mohammadi, 2012) used XFEM to simulate cohesive crack growth in FRP-retrofitted concrete beams, demonstrating the method's ability to capture debonding without mesh refinement. Similarly, (Mohammadi et al., 2013) applied XFEM to model multiple crack interactions in FRP-concrete interfaces. However, most previous studies have limitations: conventional FEM requires fine mesh around the crack tip and remeshing for crack propagation, which is computationally expensive. Additionally, interface elements often require predefined crack paths, which is not realistic. XFEM overcomes these limitations by enriching nodal degrees of freedom, allowing crack propagation through arbitrary paths without mesh modification. Despite these advantages, few studies have systematically investigated the combined effects of concrete strength, CFRP thickness, and notch geometry on the complete P-CMOD response using XFEM.

3. Numerical Analysis Methodology

The failure behavior and initial crack propagation of CFRP-reinforced notched concrete beams were numerically investigated in this study using FEA and ABAQUS software (Manual, 2012). Accordingly, a three-dimensional concrete beam reinforced in the tension (bottom) surface with a CFRP composite sheet was modeled with the mechanical properties expressed in Table 1. It should be noted that the modeled beams were plain concrete beams without internal steel reinforcement. This simplification was intentional to isolate the flexural contribution of the externally bonded CFRP sheet and to validate the XFEM crack propagation mechanism without the confounding effects of steel-concrete interaction. The beam is simple and subjected to a three-point load at the center of the beam span, as shown in Figure 1. The geometry and characteristics of the beam model were selected based on the literature for the purpose of simulations. The length (L), width (b_c), and height (h_c) of the concrete beam were 800 mm, 150 mm, and 200 mm, respectively. The length (L_f), width (b_f), and thickness (t_f) of the composite sheet were also 800 mm, 50 mm, and 0.16 mm, respectively. The density and elastic modulus of concrete were input into the model with values of 2380 kg/m^3 and 30 GPa. The numerical predictions were compared with the experimental results obtained in this study, and therefore the accuracy of the numerical modeling was confirmed. Then, results were presented for other numerical analysis cases.

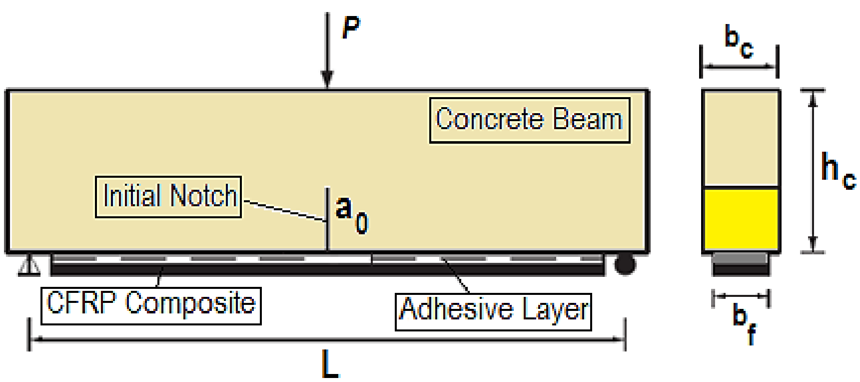

Figure 1. CFRP-strengthened concrete beam geometry with boundary conditions (pinned left, roller right) and 3point loading

Table 1. Mechanical properties of CFRP in the modeling software

Properties	CFRP
Modulus of Elasticity, GPa	240
Tensile Strength, GPa	3.90
Ultimate Strain, %	1.71
Poisson’s Ratio	0.20

In ABAQUS, solid and shell elements are the two main types of finite elements used to model different structures and behaviors. Therefore, solid, shell, and cohesive elements were used to model the concrete beam, CFRP sheet, and adhesive layer, respectively. It was assumed that CFRP exhibits linear behavior, meaning that the stress-strain curve is linear up to the point of failure, where the material loses its ultimate capacity. A concrete damaged plasticity (CDP) model was used to simulate the failure behavior of concrete caused by cracking in compression or tension. The Concrete Damaged Plasticity (CDP) model parameters were defined as follows: dilation angle ψ=31°, eccentricity ε=0.1, ratio of initial equibiaxial compressive yield stress to uniaxial compressive yield stress σ_{b0}/σ_{c0} = 1.16, ratio of the second stress invariant on the tensile meridian K_c = 0.667, and viscosity parameter μ = 0.0001. The compressive damage variable (d_c) and tensile damage variable (d_t) were defined based on the inelastic strain values, following the default Abaqus formulation for uniaxial compression and tension. In addition, in the Abaqus software, a variety of cohesive elements are used to model the behavior of bond and interface interactions between different materials. These elements can simulate the damage and separation processes at interfaces. As such, COH3D8 element, which is a three-dimensional eight-node adhesive element, was utilized. Modeling of concrete, CFRP, and adhesive layer is shown in Figure 2. Cohesive elements (COH3D8) were selected for the adhesive layer because they can simulate the initiation and propagation of debonding at the CFRP-concrete interface. This is critical because interfacial debonding is a primary failure mode in externally bonded FRP systems. The cohesive parameters (maximum normal stress σ_{max} = 3.5 MPa, shear stress τ_{max} = 4.2 MPa, and mixed-mode fracture energy G_c = 0.45 N/mm) were determined based on push-out test results reported in the literature.

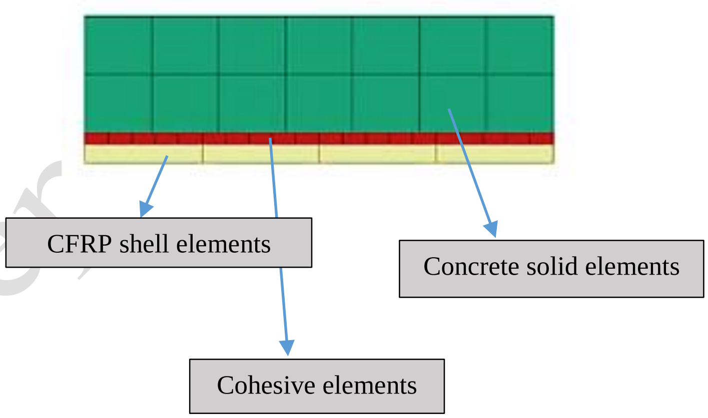

Figure 2. Model of concrete, CFRP, and adhesive layer with relevant elements

XFEM, as one of the efficient crack modeling methods in ABAQUS, was used to simulate cracking in the present study. In this method, the existence of discontinuities such as cracks in an element can be modeled through enrichment functions, where the enriched elements represent the crack growth. In particular, XFEM can continuously monitor the location of crack propagation. The crack opening criterion is assumed to be the maximum stress, so that crack propagation occurs when the maximum stress exceeds the tensile strength of the concrete. The behavior of concrete in tension and compression was considered according to Figure 3. It was also assumed that the CFRP behavior remained linearly elastic until the moment of failure.

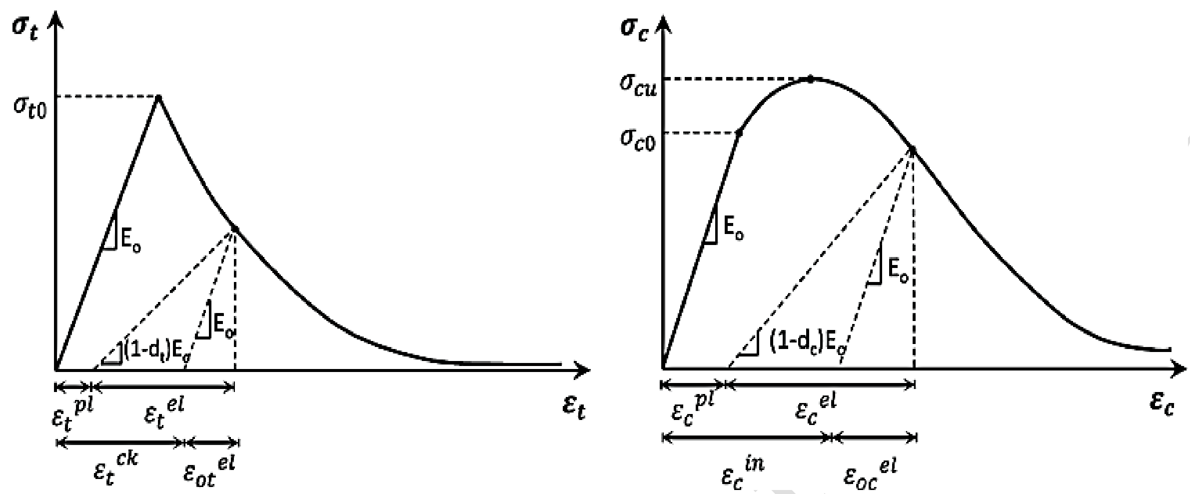

Figure 3. Constitutive model of concrete in tension and compression (Manual, 2012)

Regarding the adhesive layer, various forms of concrete softening curves have been presented in the literature. In the present study, the strain softening curve of concrete under uniaxial tension, which is used to develop the CDP model, was adopted as shown in Figure 4.

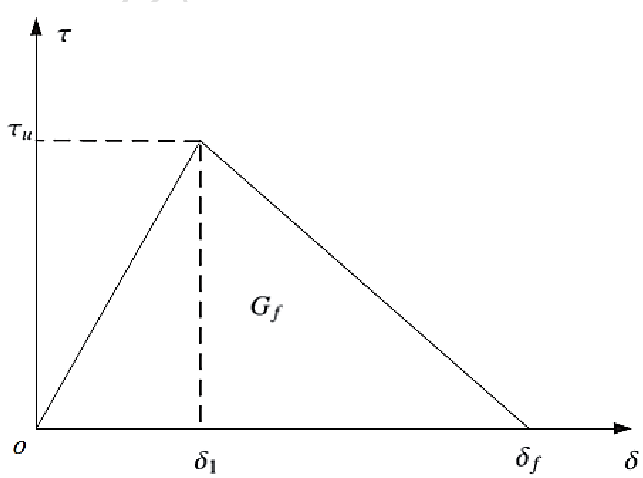

Figure 4. Bilinear local bond-slip model for CFRP-concrete interface (Manual, 2012)

In the XFEM approach, traction-separation damage laws are used to define material properties, one of which is the maximum principal stress damage. In this section, the maximum tensile stress, or in other words, the tensile strength of concrete was defined. As mentioned earlier, when the element stress exceeds the maximum stress, opening and consequently splitting occur, indicating crack propagation. The ultimate stress and strain of CFRP were considered and then mechanical properties were assigned. The material behavior for the interaction zone was selected as cohesive and according to the traction-separation rules in ABAQUS software, the ultimate stress and failure energy were assigned to the interaction zone of concrete and CFRP sheet, so that with the increase of the stress and energy of each element beyond the failure limit, the element is unable to withstand the applied stresses and failure occurs. Regarding the definition of the interaction between the concrete layer and the CFRP sheet, adhesive elements were "tied" to the solid concrete elements and the CFRP shell on each upper and lower face. For the analysis of CFRP-reinforced concrete beams, structural meshes with hexagonal (hexahedral) elements are preferred due to their uniformity and computational efficiency, especially in areas with regular geometry. In this study, a structured mesh with hexahedral and tetrahedral elements was used in some places. Hexahedral elements were used in the central region of the beam (beneath the loading point and around the notch) where stress gradients are high and uniform stress distribution is expected. These elements provide higher accuracy with fewer degrees of freedom. Tetrahedral elements were employed in regions further from the notch and near the beam ends, where stress gradients are lower. This hybrid meshing strategy balances computational efficiency with solution accuracy.

To ensure mesh independence of the numerical results, a mesh sensitivity analysis was performed using three different global element sizes: 15 mm (coarse), 10 mm (baseline), and 5 mm (fine). The maximum load differences between the coarse and baseline meshes was 5.8%, while the difference between the baseline and fine meshes was only 1.7%. Since the 5 mm mesh increased computational cost by approximately 180% without notable improvement in accuracy, the 10 mm mesh was deemed optimal and adopted for all subsequent parametric analyses.

For all nonlinear finite element analyses, convergence was achieved when the residual force norm was less than 0.5% of the applied force norm (default Abaqus criterion). Additionally, the displacement correction norm was monitored with a tolerance of 0.01 mm. The maximum number of iterations per increment was set to 20, with an automatic incrementation scheme. A minimum increment size of 10^{-6} was specified to capture snap-through behavior and sudden load drops during crack propagation.

4. Validation of Numerical Approach

To validate the numerical results, two analytical and numerical studies were selected and the load-CMOD diagrams were compared, as shown in Figure 5. The first example was the study by Wu et al. (Wu et al., 2013). For the verification model of Wu et al. (2013), the concrete beam had dimensions of 700mm×150mm×150mm(L×b×h) with a notch-to-height ratio of 0.3. The concrete compressive strength was 35 MPa, elastic modulus 28 GPa, and tensile strength 2.8 MPa. The CFRP sheet had a thickness of 0.15 mm, width of 50 mm, elastic modulus 230 GPa, and tensile strength 3.5 GPa. Based on the comparison of the results, the proposed model can well simulate the elastic section of the diagram and especially the post-crack behavior of the strengthened beam.

The percentage difference between the two models in the ultimate load value is 1.8%, with values of 8.94 kN and 8.78 kN in the analytic model and the present study, respectively.

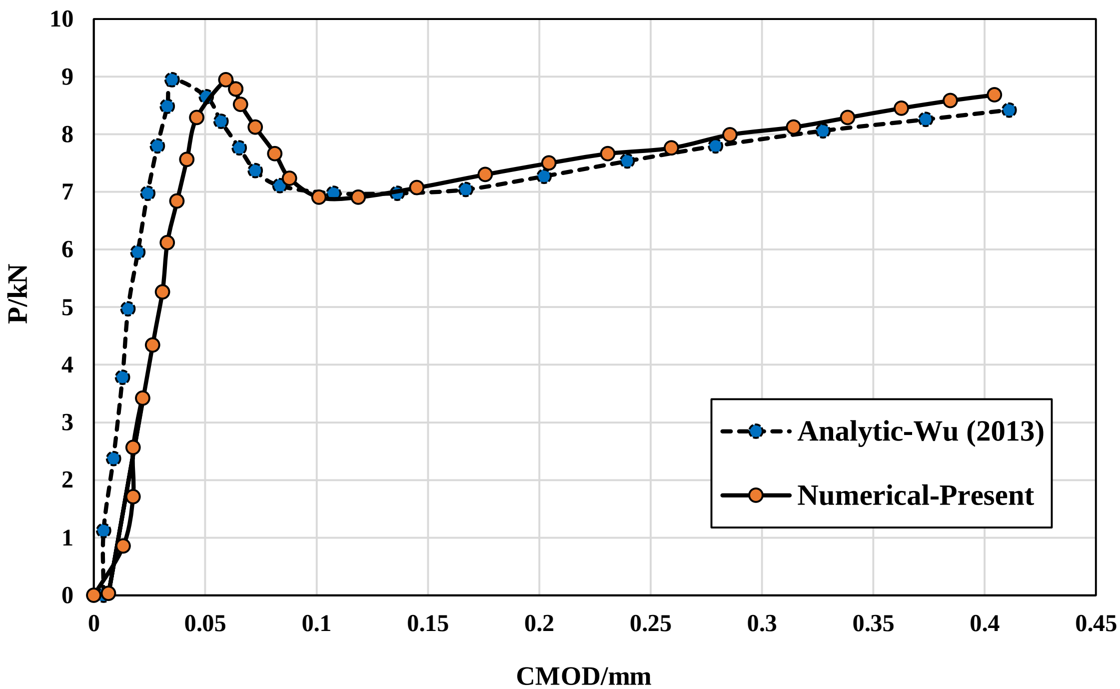

Figure 5. Comparison of results of analytical model in Wu et al. (Wu et al., 2013) and the present study

In the second validation example, the results were compared with the FEM of Zheng et al. (Zheng et al., 2016). For the verification model of Zheng et al. (2016), the beam dimensions were 800 mm × 100 mm × 200 mm with a notch-to-height ratio of 0.4. Concrete compressive strength was 40 MPa, elastic modulus 30 GPa, and CFRP thickness 0.17 mm with elastic modulus 240 GPa. The small discrepancies (1.8% and 5.16%) between the present model and the reference studies can be attributed to several factors: (1) differences in the assumed tensile strength and fracture energy of concrete, which are not always reported in detail; (2) variations in the interfacial bond-slip parameters for the CFRP-concrete interface; and (3) the inherent variability in experimental measurements. Regarding crack patterns, the present XFEM simulations produced a single dominant flexural crack initiating from the notch tip and propagating vertically toward the compression zone. This matches the crack patterns reported in both Wu et al. (2013) and Zheng et al. (2016), where no significant shear cracks or secondary cracking were observed due to the three-point bending configuration with a sufficiently large shear span-to-depth ratio. The load-CMOD diagram was considered to compare the results according to Figure 6. As it is seen from the comparison of the results, the proposed model can well simulate the elastic part and especially the post-crack behavior of the strengthened concrete beam. The percentage difference between the two models in the ultimate load value is 5.16%, with values of 13.03 kN and 12.39 kN in Zheng et al. (Zheng et al., 2016) model and present models, respectively.

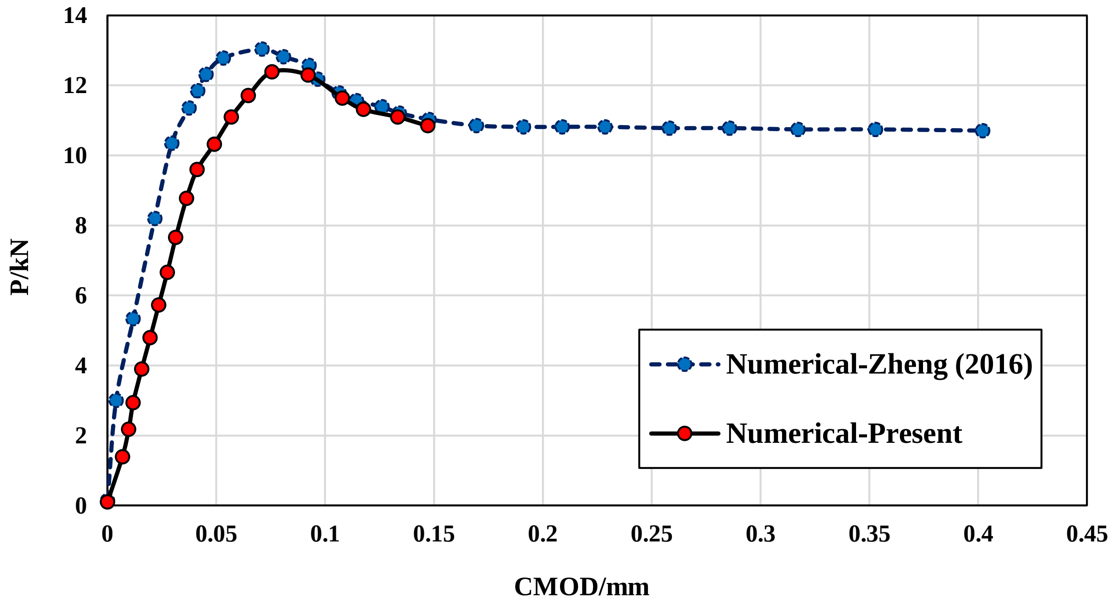

Figure 6. Comparison of results of analytical model in (Zheng et al., 2016) and the present study

5. Parametric Analysis Results

The examined parameters in this section include the effects of concrete compressive strength, CFRP sheet thickness, notch-to-beam height ratio, as well as a comparison between the two cases of beams with and without CFRP strengthening on the P-CMOD curves of the beams under center-point load. The P-CMOD curve is an essential tool for evaluating the performance of concrete beams strengthened with CFRP sheets. This curve shows the relationship between the applied load and the corresponding crack opening displacement, highlighting the different stages of loading and failure. The parametric parameters selected (concrete compressive strength: 20, 40, 60 MPa; CFRP thickness: 0.1, 0.16, 0.2 mm; notch-to-height ratio: 0.2, 0.3, 0.4) were chosen based on common ranges found in practice and in accordance with ACI 440.2R-17 guidelines for externally bonded FRP systems. Concrete strengths of 20-60 MPa cover normal to high-strength concrete. CFRP thicknesses of 0.1-0.2 mm represent single to double layers of typical commercially available sheets. Notch ratios of 0.2-0.4 simulate various levels of pre-existing damage. While parameters such as CFRP length, sheet width, and fiber orientation (layup configuration) are also influential, they were beyond the scope of this study due to computational constraints. Future research should systematically investigate these additional parameters.

5.1 Effect of concrete compressive strength

Concrete strength plays an important role in determining the behavior of the P-CMOD curve for RC beams, especially beams reinforced with CFRP sheets. Changes in concrete strength can significantly affect crack initiation, propagation, and overall load-bearing capacity. Figure 7 shows the variations in P-CMOD curve as the compressive strength of concrete beam is increased. It can be seen that the effect of concrete strength on the P-CMOD curve is significant. In this regard, beams with lower concrete strength, i.e. 20 MPa, show lower capacities. In these types of beams, the initial slope of the curve is lower, indicating lower stiffness. Therefore, cracks form at lower loads, leading to an initial point of nonlinearity in the curve. Regarding the post-cracking behavior, P-CMOD curve shows a rapid decrease in load capacity, as the concrete fails before reaching a significant deformation. Beams with medium concrete strength indicate improved stiffness and load-bearing capacity. In this case the CFRP sheet starts to engage effectively, allowing for a more controlled transfer of tensile loads. As such, the ultimate load capacity is higher compared to low-strength concrete and gradually decreases after the peak due to the combined contribution of concrete and CFRP. The high-strength concrete offers superior compressive and tensile properties. The curve indicates high stiffness and load-bearing capacity. Higher loads are required to initiate cracking, leading to a significant increase in the first peak load in the curve. The ultimate load capacity is maximized and often reaches higher values due to the elasticity of the concrete, while the CMOD gradually increases as the cracks spread. CFRP has optimal performance and allows for controlled deformation before failure.

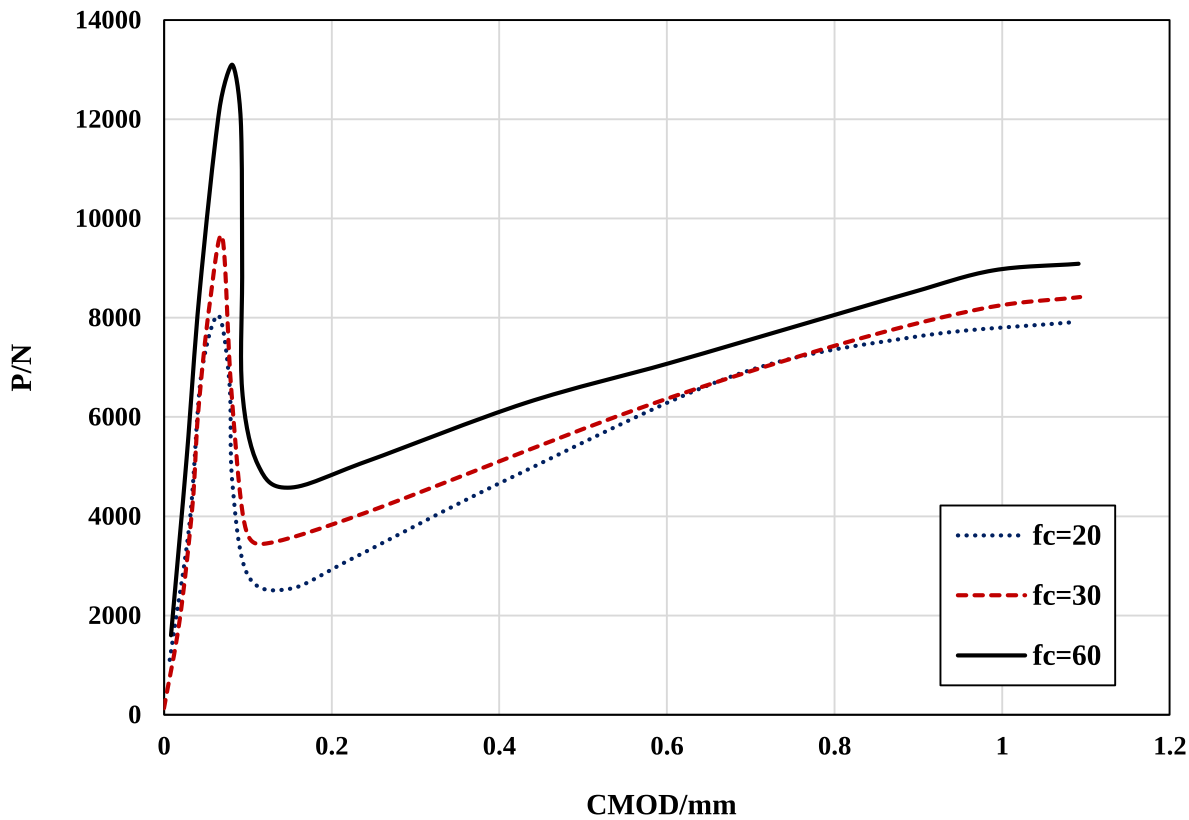

Figure 7. Effect of concrete compressive strength on P-CMOD curve

5.2 Effect of CFRP sheet thickness

The results of the effect of CFRP sheet thickness (h_f) are shown in Figure 8. It can be seen that the load capacity is increased as the CFRP thickness is increased. This occurs because a thicker CFRP sheet requires a greater tension force for a certain CMOD. In this respect, when the sheet thickness (h_f) increases from 0.1 mm to 0.2 mm, the peak load rises from 8.62 kN to 10.44 kN which shows an increase of 21%. Although the increase in the thickness of the CFRP sheet has a trivial effect of the first maximum load in the P-CMOD curve, it can be seen that the ultimate load increases sharply as the CFRP sheet thickness is increased. This is indicative of the fact that the first maximum load is basically dependent on the performance of the concrete beam and the loss of concrete strength, while the ultimate load is critically related to the activation of the CFRP sheet when exposed to tensile loads after the concrete damage and localized cracking. In this case, when the sheet thickness (h_f) increases from 0.1 mm to 0.2 mm, the ultimate load rises from 6.27 kN to 10.53 kN which shows an increase of 68%.

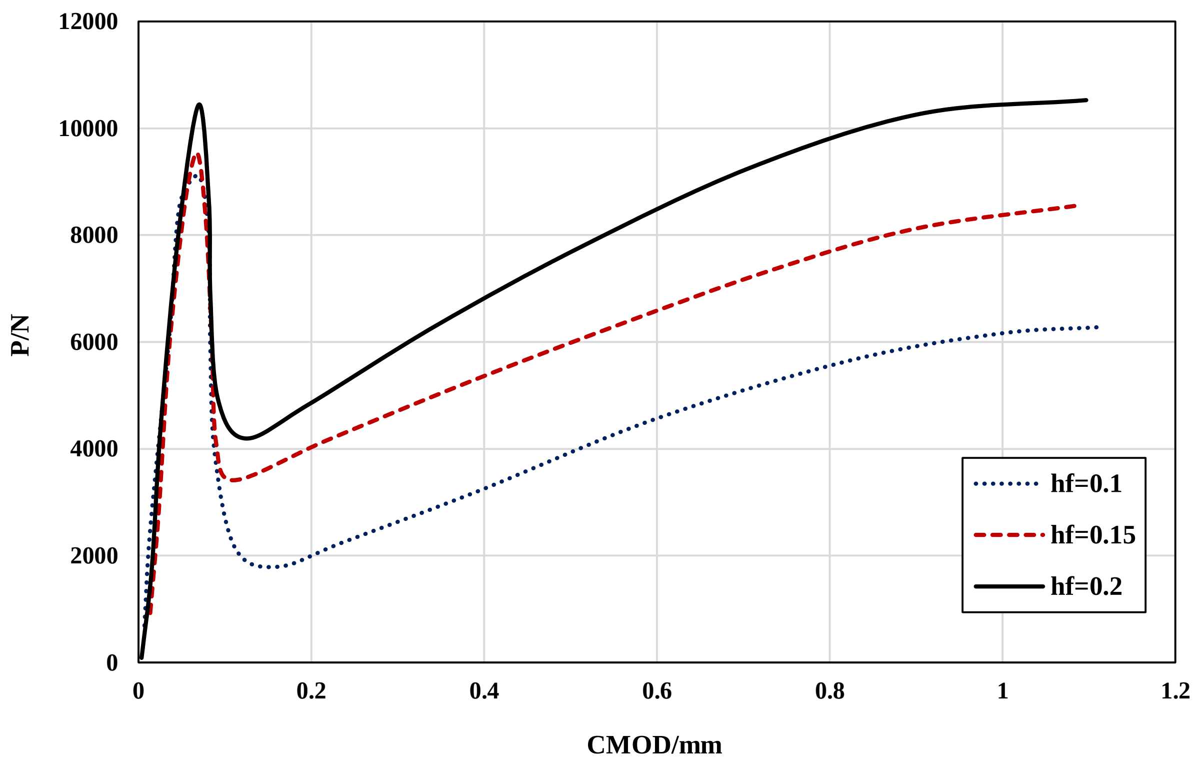

Figure 8. Effect of CFRP thickness on P-CMOD curve

5.3 Effect of notch-to-beam height ratio

In this section, the beam height is kept constant as h_c= 200 mm and the notch height (a_0) is increased from 40 mm to 60 mm and 80 mm. According to Figure 9, the results of different a_0/h_c ratios show that load-bearing capacity of the beam increases with increasing notch height.

Accordingly, as the notch height is increased, the first maximum load decreases sharply but the ultimate load does not vary significantly. The reason is that larger initial notch heights lower the bearing capacity of the retrofitted beam, whereas after the first crack, unstable cracks begin to extend. As a consequence, the ultimate load depends only on the capacity of CFRP sheet. In detail, by increasing a_0 from 40 to 60 mm, the first maximum load decreases by 34% but the ultimate load is reduced by 9%.

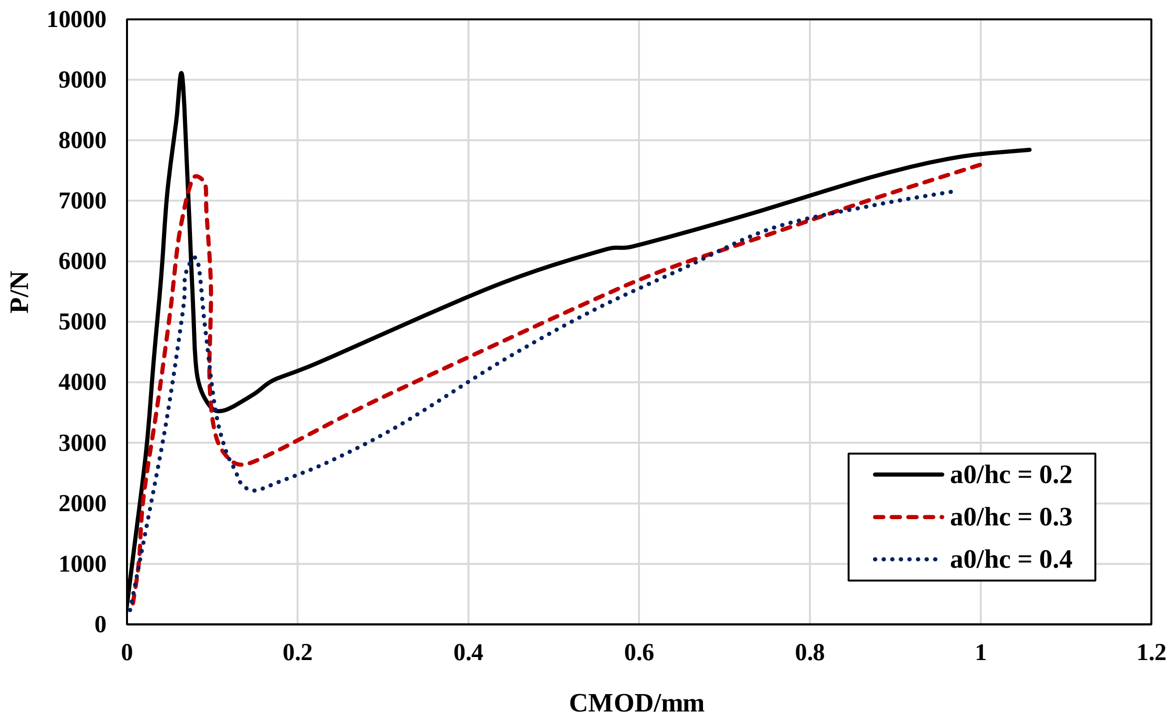

Figure 9. Effect of notch-to-beam height ratio on P-CMOD curve

The higher the initial notch height, the closer it is to the tensile surface of the beam. Therefore, the initial elasticity may be similar to the short notch condition, but as the notch height approaches critical threshold, the elasticity decreases. The 'critical threshold' in fracture mechanics refers to the notch-to-beam height ratio beyond which the beam's behavior transitions from ductile to brittle or where the failure mode changes from concrete crushing to CFRP debonding. For the present geometry, this threshold occurs approximately at $a_0/h_c = 0.35$. Below this value, the beam exhibits significant post-cracking ductility with gradual load decay; above this value, the initial notch is so deep that the remaining ligament cannot sustain significant plastic deformation, leading to a sharper load drop after the first peak. It can also be concluded that more loads are required before significant cracking occurs, which leads to more energy absorption before failure as the area under the P-CMOD curve is increased. In addition, in larger a_0/h_c ratios, this beam reaches a higher maximum load due to better stress distribution compared to beams with lower a_0/h_c ratios.

5.4 Ductility assessment of retrofitted beams

Ductility, defined as the ability to undergo inelastic deformation without significant loss of load capacity, is a critical performance indicator for retrofitted structures. Using the displacement ductility index $\mu = \Delta_u/\Delta_y$, where Δ_u is the displacement at ultimate load and Δ_y is the displacement at yield (first peak load), the following observations were made.

For non-strengthened beams (a_0/h_c=0.3), μ was approximately 1.8, indicating brittle failure. In contrast, CFRP-strengthened beams exhibited μ values ranging from 4.2 to 6.5, depending on CFRP thickness. Increasing CFRP thickness from 0.1 mm to 0.2 mm enhanced μ by approximately 55%. Furthermore, beams with higher concrete strength (60 MPa) showed lower ductility ($\mu \approx 4.0$) but higher ultimate load, whereas lower strength concrete (20 MPa) showed higher ductility ($\mu \approx$ 6.5) with reduced load capacity. This trade-off between strength and ductility should be considered in practical retrofitting design.

5.5 Effect of strengthening beam with CFRP sheet

Figure 10 shows the difference between the results of concrete beam with and without CFRP strengthening. The elastic region shows the linear relationship between load and displacement. At this stage, the beam behaves elastically, meaning that any deformation is reversible. The second phase is characterized by a sudden increase in CMOD with relatively small changes in load. The concrete begins to lose its tensile strength, but the CFRP sheet begins to absorb some of the tensile forces. In the third stage, the load continues to increase and the CMOD increases more rapidly. The performance of the CFRP sheet becomes very important at this stage, as it helps to distribute the stresses and prevent sudden failure. This is why the displacement values change much more than the load. Nevertheless, beams with no CFRP strengthening show almost similar peak loads but the descending branch of the P-CMOD curve is sharp with brittle failure. However, the beams with CFRP strengthening represent an ascending branch after the first maximum load is experienced. The hardening part of the curve is because of the CFRP sheet contribution, which leads to higher displacements. In this regard, the difference between the strengthened (S) and non-strengthened (NS) beams in terms of first peak load and ultimate displacement in models with a_0/h_c = 0.3 is respectively 20% and 733%. This shows the effectiveness of strengthening concrete beams with CFRP sheets.

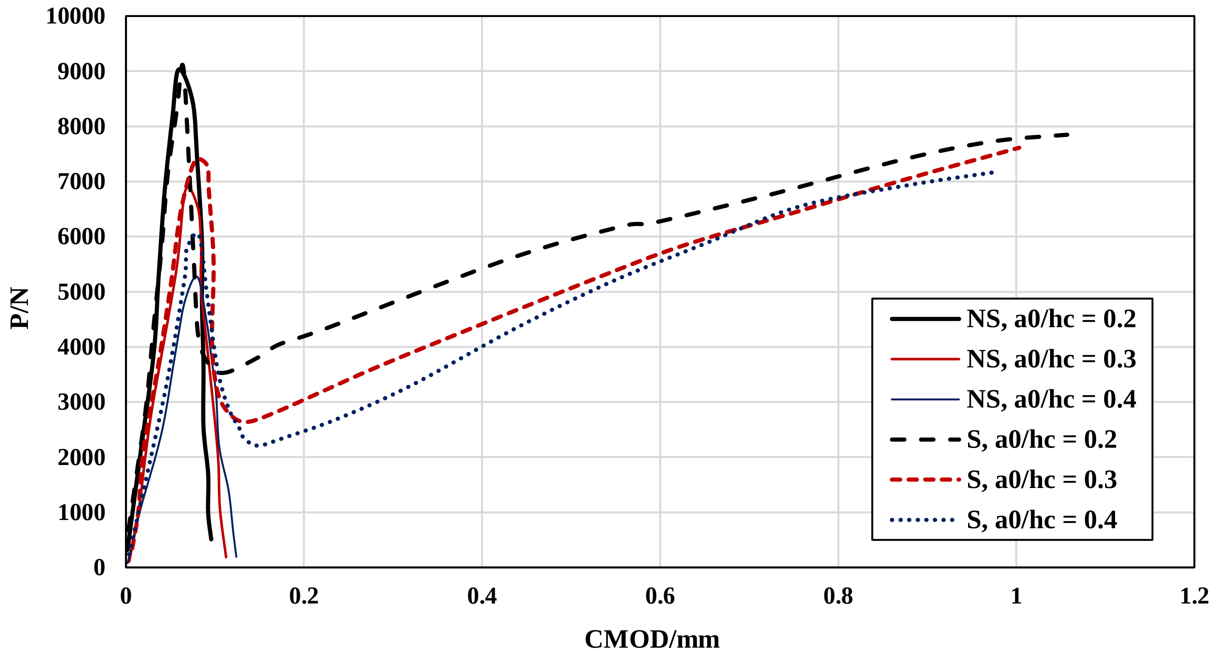

Figure 10. Effect of strengthening concrete beam with CFRP sheet on P-CMOD curve

5.6 Failure mechanism analysis based on stress and strain distribution

To gain deeper insight into the failure mechanism, stress and strain distributions at the final loading stage were examined. Figure 8 presents the von Mises stress contour in the concrete beam, the maximum principal stress distribution in the CFRP sheet, and the crack propagation path predicted by XFEM for a beam with $h_f = 0.16$ mm and $a_0/h_c = 0.3$. The analysis reveals a three-stage failure process. Stage I (elastic): The notch tip experiences stress concentration, with tensile stress reaching approximately 2.5 MPa, just below the concrete tensile strength. Stage II (crack initiation and CFRP activation): Once the principal stress exceeds concrete tensile strength (3.0 MPa), a flexural crack initiates at the notch tip. Concurrently, tensile stresses in the CFRP sheet rise sharply from near-zero to approximately 1.2 GPa, indicating load transfer from concrete to CFRP. Stage III (debonding propagation and final failure): As the crack propagates toward the compression zone, interfacial shear stresses at the CFRP-concrete interface exceed the bond strength (≈4.5 MPa), leading to progressive debonding starting from the crack location and spreading toward the beam ends. Final failure occurs when the CFRP tensile stress reaches its ultimate strength (3.9 GPa) or when concrete crushing develops in the compression zone. This stress-based analysis confirms that the ultimate load is governed by CFRP capacity, while the first peak load is primarily controlled by concrete tensile strength. One limitation of this study is that the beam geometry (shear span-to-depth ratio = 2.67) and loading configuration (three-point bending) were selected to promote flexural failure. Therefore, the findings are primarily applicable to flexure-dominant retrofitting scenarios. The interaction between flexural cracks and shear failure mechanisms was not explicitly modeled. Future studies should extend this XFEM framework to investigate shear-critical beams and beams with combined flexural-shear failure modes.

6. Conclusions

In this study, a numerical parametric investigation was carried out using the XFEM capability in Abaqus software to assess the effect of geometrical and mechanical variations on the flexural response of CFRP-retrofitted concrete beams. Thus, the effects of concrete compressive strength, CFRP sheet thickness, notch-to-beam height ratio, and efficiency of strengthening concrete beams with CFRP is examined. The following results can be obtained.

- The effect of concrete strength on the P-CMOD curve is significant. In this regard, beams with lower concrete strength, i.e. 20 MPa, show lower capacities compared to beams with higher concrete strength, i.e., 60 MPa. Such difference is 59%.
- The load capacity is increased as the CFRP thickness is increased. This occurs because a thicker CFRP sheet requires a greater tension force for a certain CMOD. In this respect, when the sheet thickness (h_f) increases from 0.1 mm to 0.2 mm, the peak load rises from 8.62 kN to 10.44 kN"* the peak load rises from 8616 kN to 10438 kN; which shows an increase of 21%.
- Although the increase in the thickness of the CFRP sheet has a trivial effect of the first maximum load, the ultimate load increases sharply as the CFRP sheet thickness is increased. This indicates that the first maximum load is basically dependent on the performance of the concrete beam, while the ultimate load is critically related to the activation of the CFRP sheet after localized cracking in concrete. In this case, when the sheet thickness (h_f) increases from 0.1 mm to 0.2 mm, the ultimate load rises from 6.27 kN to 10.53 kN which shows an increase of 68%.
- The load-bearing capacity of the beam increases with increasing notch height. Accordingly, as the notch height is increased, the first maximum load decreases sharply but the ultimate load does not vary significantly. The reason is that larger initial notch heights lower the bearing capacity of the retrofitted beam. As a consequence, the ultimate load depends only on the capacity of CFRP sheet. In detail, by increasing a_0 from 40 to 60 mm, the first maximum load decreases by 34% but the ultimate load is reduced by 9%.

7. Acknowledgments

The authors acknowledge the use of AI-assisted language editing tools for improving the readability and grammar of this manuscript. All technical content, analysis, results, and conclusions remain the sole responsibility of the authors.

References

Ashteyat, A., Almahadin, W., Abdel-Jaber, M. t., & Almuaythir, S. (2024). Shear repairing of reinforced concrete beams exposed to high temperature using basalt fiber reinforcing bars and CFRP ropes and strips. *Composites Part C: Open Access*, *15*, 100517. https://doi.org/10.1016/j.jcomc.2024.100517

Bai, J., Yang, Y., Huang, P., Guo, X., Chen, Z., Wan-Wendner, R., & Li, W. (2024). Durability of CFRP strengthened RC beam after six years exposure to natural hygrothermal environment with sustained loads. *International Journal of Fatigue*, *181*, 108126. https://doi.org/0.1016/j.ijfatigue.2023.108126

Benaoum, F., Khelil, F., & Benhamena, A. (2020). Numerical analysis of reinforced concrete beams pre cracked reinforced by composite materials. *Fracture and Structural Integrity*, *14*(54), 282–296. https://doi.org/10.3221/IGF-ESIS.54.20

Cazacu, C. E., Dumitriu, C. Ș., & Bărbulescu, A. (2024). Concrete CFRP-Reinforced Beam Performances, Tests and Simulations. *Sustainability*, *16*(7), 2614.

DEHESTANI, M. (2020). Near free-edge stresses in FRP-to-concrete bonded joint due to mechanical and thermal loads. https://doi.org/10.24200/sci.2018.50594.1779

Duarte, P., Correia, J., Ferreira, J., Nunes, F., & Arruda, M. (2014). Experimental and numerical study on the effect of repairing reinforced concrete cracked beams strengthened with carbon fibre reinforced polymer laminates. *Canadian Journal of Civil Engineering*, *41*(3), 222–231.

Esna Ashari, S., & Mohammadi, S. (2012). Fracture analysis of FRP-reinforced beams by orthotropic XFEM. *Journal of composite materials*, *46*(11), 1367–1389.

Fan, X., Liu, J., Zou, L., & Wang, J. (2025). Numerical Simulation Study on the Fracture Process of CFRP-Reinforced Concrete. *Buildings*, *15*(15), 2636. https://doi.org/10.3390/buildings15152636

Han, Z., Gao, J., Song, H., & Xu, G. (2024). Bond properties of CFRP externally bonded reinforcement on groove in concrete. *International Journal of Concrete Structures and Materials*, *18*(1), 32. https://doi.org/10.1186/s40069-024-00678-9

Harle, S. M. (2024). Durability and long-term performance of fiber reinforced polymer (FRP) composites: A review. Structures,

Hosseini, M., Amiri, A., & Beiranvand, P. (2016). Numerical analysis of reinforced concrete beams containing bending and shear opening and strengthened with FRP sheet. *Engineering Solid Mechanics*, *4*(3), 145–152. https://doi.org/10.5267/j.esm.2016.1.003

Hu, X., Bai, T., Zhao, Y., Ren, Q., Chen, Y., Li, H., & Shi, C. (2024). Interface mechanical properties of CFRP-seawater sea sand concrete under simulated seawater immersion. *Journal of Building Engineering*, *97*, 110768. https://doi.org/10.1016/j.jobe.2024.110768

Jahami, A., & Issa, C. A. (2024). An updated review on the effect of CFRP on flexural performance of reinforced concrete beams. *International Journal of Concrete Structures and Materials*, *18*(1), 14.

Kim, J.-H., & Kim, Y. J. (2024). Structural performance of CFRP-confined RC columns under earthquake-induced fire. *Engineering Structures*, *309*, 118097. https://doi.org/10.1016/j.engstruct.2024.118097

Li, X. Q., Sun, X. Y., & Li, Y. W. (2014). Study on Three-Point Bending Numerical Tests of CFRP Reinforced Concrete Beam with Initial Crack. *Advanced Materials Research*, *838*, 639–643.

Ma, X., Guo, T., Xing, Y., Qin, R., Long, H., Bao, C., Cao, F., & Hong, R. (2025). Study on Seismic Behavior of Earthquake-Damaged Joints Retrofitted with CFRP in Hybrid Reinforced Concrete–Steel Frames. *Materials*, *18*(21), 4857. https://doi.org/10.3390/ma18214857

Manual, A. S. U. s. (2012). Abaqus 6.11. *http://130.149*, *89*(2080), v6.

Mercimek, Ö., Anıl, Ö., Akkaya, S. T., Erdem, R. T., Çelik, A., Kopraman, Y., & Abukan, A. (2025). Experimental behavior of shear deficient RC beams strengthened with CFRP strips against reversible cyclic earthquake load. *Structural Concrete*.

Mofid, T., & Tavakoli, H. (2020). Experimental investigation of post-earthquake behavior of RC beams. *Journal of Building Engineering*, *32*, 101673.

Mofid, T., & Tavakoli, H. (2021). Experimental Investigation of Cyclic Degradation of Light RC Beams under Periodic Loading. *Journal of Structural and Construction Engineering*, *8*(Special Issue 2), 243–263.

Mofid, T., & Tavakoli, H. (2023). Experimental investigation of mechanical behavior of lightweight RC elements under repeated loadings. Structures,

Mohammadi, T., Wan, B., & Harries, K. (2013). Intermediate crack debonding model of FRP-strengthened concrete beams using XFEM. SIMULIA Community Conf., Dassault Systèmes, Paris,

Paul, S. K., & Sahu, P. (2020). Finite element analysis of retrofitting of Rc Beam with CFRP using Abaqus. *International Research Journal of Engineering and Technology (IRJET)*, *7*(2), 1268–1273.

Saeidi Googarchin, H., & Bidadi, J. (2025). Experimental evaluation of residual tensile properties of CFRP-aluminum butt adhesive joints subjected to systematic creep damage. *Polymer Composites*, *46*(9), 8318–8335. https://doi.org/10.1002/pc.29495

Sakbana, A., & Mashreib, M. (2020). Finite element analysis of CFRP-reinforced concrete beams. *Revista ingeniería de construcción*, *35*(2), 148–169.

Salih, R., & Zhou, F. (2019). Numerical investigation of the behavior of reinforced concrete beam reinforced with FRP bars. *Civil Engineering Journal*, *5*(11), 2296–2308. https://doi.org/10.28991/cej-2019-03091412

Samadvand, H., & Dehestani, M. (2020). A stress-function variational approach toward CFRP-concrete interfacial stresses in bonded joints. *Advances in concrete construction*, *9*(1), 43–54. https://doi.org/10.12989/acc.2020.9.1.043

Satyanarayana, A. (2025). Advanced Structural Enhancement of Bridges: ANSYS Simulation, CFRP Retrofitting Techniques, and Fuzzy Logic Integration. *Civil Engineering Infrastructures Journal*.

SD, A. K., & Pratap, B. (2025). Analysis of Fiber Bragg Grating Sensor for CFRP Beam Crack Growth. *Civil Engineering Infrastructures Journal*.

Shardakov, I., Shestakov, A., Glot, I., & Bykov, A. (2016). Process of cracking in reinforced concrete beams (simulation and experiment). *Fracture and Structural Integrity*, *10*(38), 339–350. https://doi.org/10.3221/IGF-ESIS.38.44

Sinaei, H., Jumaat, M. Z., & Shariati, M. (2011). Numerical investigation on exterior reinforced concrete Beam-Column joint strengthened by composite fiber reinforced polymer (CFRP). *Int. J. Phys. Sci*, *6*(28), 6572–6579. https://doi.org/10.5897/IJPS11.1225

Tran, H., Nguyen-Thoi, T., & Dinh, H.-B. (2025). State-of-the-art review of studies on the flexural behavior and design of frp-reinforced concrete beams. *Materials*, *18*(14), 3295.

Wu, Z.-M., Fan, X.-L., Zheng, J.-J., & Wu, X. (2013). Modeling of debonding and fracture process of FRP-strengthened concrete beams via fracture mechanics approach. *Journal of reinforced plastics and composites*, *32*(22), 1733–1745. https://doi.org/10.1177/0731684413501569

Zhang, J., Yang, J., & Yu, T. (2026). Durability of FRP bars and FRP-reinforced concrete beams: A critical review of accelerated aging tests and performance insights. *Composites Part B: Engineering*, *308*, 112965. https://doi.org/10.1016/j.compositesb.2025.112965

Zhang, P., Li, H., Liu, Y., Tao, X., Qi, Y., & Sheikh, S. A. (2025). Interfacial bonding performance of CFRP sheet reinforced corroded steel plates under fatigue loading. *Construction and Building Materials*, *468*, 140450. https://doi.org/10.1016/j.conbuildmat.2025.140450

Zhang, W., Yu, X., & Jiang, C. (2024). Flexural reliability of corroded RC beams strengthened with CFRP sheets considering longitudinal corrosion non-uniformity of steel bars. *Journal of Building Engineering*, *97*, 110888. https://doi.org/10.1016/j.jobe.2024.110888

Zheng, J.-J., Dai, J.-G., & Fan, X.-L. (2016). Fracture analysis of frp-plated notched concrete beams subjected to three-point bending. *Journal of Engineering Mechanics*, *142*(3), 04015096. https://doi.org/10.1061/(ASCE)EM.1943-7889.0001021